Polarization-dependent optical 2D Fourier transform spectroscopy of semiconductors

Tianhao Zhang[†‡], Irina Kuznetsova[§], Torsten Meier[§], Xiaoqin Li[†¶], Richard P. Mirin[‖], Peter Thomas[§], and Steven T. Cundiff[†,††]

[†]JILA, University of Colorado and National Institute of Standards and Technology, Boulder, CO 80309-0440; [‡]Department of Physics, University of Colorado, Boulder, CO 80309; [§]Department of Physics and Material Sciences Center, Philipps University, Renthof 5, D-35032 Marburg, Germany; and [‖]National Institute of Standards and Technology, Boulder, CO 80305

Edited by Robin M. Hochstrasser, University of Pennsylvania, Philadelphia, PA, and approved May 31, 2007 (received for review February 23, 2007)

Optical 2D Fourier transform spectroscopy (2DFTS) provides insight into the many-body interactions in direct gap semiconductors by separating the contributions to the coherent nonlinear optical response. We demonstrate these features of optical 2DFTS by studying the heavy-hole and light-hole excitonic resonances in a gallium arsenide quantum well at low temperature. Varying the polarization of the incident beams exploits selection rules to achieve further separation. Calculations using a full many-body theory agree well with experimental results and unambiguously demonstrate the dominance of many-body physics.

excitons | many-body effects | ultrafast

Optical excitation of a direct gap semiconductor, such as gallium arsenide (GaAs), produces electron-hole pairs. The Coulomb attraction between the electron and hole can result in a bound state, known as an exciton, with a hydrogenic wavefunction for the relative coordinate. Excitons have a large oscillator strength because of the proximity of the electron and hole and thus can dominate the absorption spectrum close to the fundamental band gap. In GaAs heterostructures, the exciton binding energy is of order 10 meV; thus, excitonic resonances appear only at low temperatures. Excitons and unbound electron-hole pairs exhibit dynamics on a femtosecond-to-picosecond time scale. These timescales, combined with the strong interaction with light, make ultrafast spectroscopy an ideal tool for studying carrier dynamics in semiconductors.

Over the last two decades, excitonic resonances in semiconductors have been studied extensively by using ultrafast spectroscopy, primarily transient four-wave-mixing (TFWM) (1, 2). The measurements clearly showed signatures of many-body effects. The first and most prominent was a signal for the "wrong" time delay in a two-pulse TFWM experiment. Theoretically, such signals could arise from several effects including local fields (3, 4), biexcitons (5), excitation-induced dephasing (6, 7), or excitation-induced shift (8). Time resolving the signal also provided evidence for many-body contributions (9, 10), although it did not resolve the ambiguity regarding the underlying phenomena.

Recent results using optical 2D Fourier transform spectroscopy (2DFTS) to study the exciton resonances have shown that much more information is obtained, promising a more stringent test of the theory (11). 2DFTS traces its roots to NMR (12). Recently, there has been significant progress in translating multidimensional NMR techniques into the infrared and optical domains for the study of vibrations (13) and electronic excitations (14–16) in molecules. Although the usefulness of adding a second dimension was recognized in TWFM studies of semiconductors (17–20), only the intensity of the emitted signal, not the phase-resolved electric field, was measured. The transient absorption experiments clearly show that detecting only the real part of the emitted field is advantageous (21, 22), but the effects of inhomogeneous broadening cannot be removed. 2DFTS combines the best features of both, resolving the signal into real and imaginary parts while simultaneously being able to extract the underlying physics despite the presence of inhomogeneity caused by structural disorder.

Here, we present an experimental and theoretical study of the polarization dependence of the real part of the optical 2DFTS of the excitonic resonances in a semiconductor multiple quantum well. The theoretical results are based on a many-body theory including correlations at a microscopic level with parameters chosen to match the experiments. Previous experimental results were compared with a phenomenological theory (11, 23), or only the magnitude spectra were considered (24). Theoretical results without comparison to experiment have also recently been presented (25). Our results show good agreement between experiment and theory, including the dependence on laser tuning. Calculations with the full theory as compared with just Pauli blocking or the Hartree–Fock approximation clearly demonstrate the essential role of the many-body correlations, which is particularly clear for cocircular-polarized excitation. Cross-linear excitation suppresses single-exciton resonances and reveals contributions caused by biexciton correlations.

Optical 2DFTS is based on three-pulse TFWM with two important improvements: the signal is heterodyne detected against a fixed-phase local oscillator, and the delay between the excitation pulses is stepped with subwavelength precision. These two features allow the phase of the emitted signal to be correlated with the phase delay between the excitation pulses by taking a 2D Fourier transform. The resulting spectrum unambiguously shows coupling between resonances as a "cross-peak." Furthermore, with the help of an auxiliary experiment, it is possible to separate the signal into real and imaginary parts. Although the two-pulse version of TFWM has been used extensively to study excitonic resonances in semiconductors (1–10, 17–20, 26–28), the three-pulse configuration has been used in only a handful of cases. TFWM experiments have also been performed in which the emitted signal was characterized by using a variety of techniques beyond simple temporal or spectral resolution (26–28); however, changes in the overall phase of the signal were not measured, nor were they correlated with the phase of the excitation pulses.

Materials and Methods

Experiment. The experimental geometry is shown in Fig. 1. Three incident 100-fs pulses are produced by a mode-locked Ti:sapphire laser at a repetition rate of 76 MHz and a wavelength of ≈800 nm (tunable). They have wavevectors $\mathbf{k}_a$, $\mathbf{k}_b$, and $\mathbf{k}_c$ and are

Author contributions: T.Z., T.M., X.L., P.T., and S.T.C. designed research; T.Z., I.K., and X.L. performed research; R.P.M. contributed new reagents/analytic tools; I.K. and T.M. analyzed data; and S.T.C. wrote the paper.

The authors declare no conflict of interest.

This article is a PNAS Direct Submission.

Abbreviations: 2DFTS, 2D Fourier transform spectroscopy; TFWM, transient four-wave-mixing; SRDT, spectrally resolved differential transmission; hh, heavy hole; lh, light hole.

[¶]Present address: Department of Physics, University of Texas, Austin, TX 78712-0264.

[††]To whom correspondence should be addressed. E-mail: cundiffs@jila.colorado.edu.

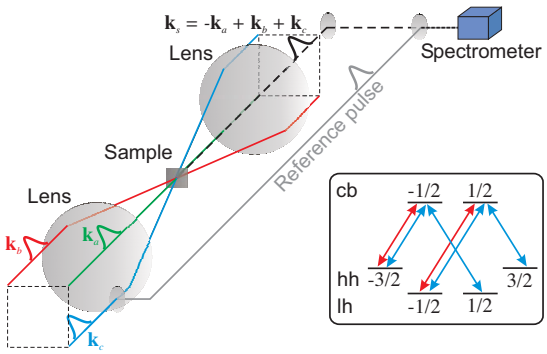

Fig. 1. Experimental setup. (*Inset*) The magnetic substates of the conduction band (cb) and hh and lh valence bands. Transitions driven by cocircular-polarized excitation are shown by red arrows, and those for linear-polarized excitation are shown by blue arrows.

arranged on three corners of a square, with $\mathbf{k}_b$ and $\mathbf{k}_c$ on one diagonal. Passing the beams through a single lens causes them to overlap at the focus, where the sample is positioned. The nonlinear interaction of the beams in the sample produces wave-mixing signals, with the TFWM signal caused by all three beams going in direction $-\mathbf{k}_a + \mathbf{k}_b + \mathbf{k}_c$, which is the fourth corner of the square. If $\mathbf{k}_a$ arrives first in time, the conjugation of the phase evolution between the first and third time periods reverses the dephasing because of inhomogeneous broadening and produces a photon echo signal. Thus we refer to this time ordering as a "rephasing" excitation sequence. One advantage of using three excitation pulses is that the time ordering of the first two pulses can be interchanged. For a homogeneously broadened system, this still produces a TFWM signal. However, the phase evolution is not reversed for this "nonrephasing" excitation sequence, so a photon echo is not produced in an inhomogeneously broadened system. Comparison of the spectra for rephasing and nonrephasing excitation gives insight into the presence of inhomogeneity and allows isolation of Liouville-space pathways (11, 29). We designate the time between first two pulses as τ, the time between the second and third pulses as T, and the time after the third pulses as t. This complex-valued signal is designated $S(\tau, T, t)$ in the time domain.

After passing through the sample, the beams, including the signal, are recollimated by a second lens. The signal is combined with a reference beam on a beam splitter. The combined signal and reference are coupled into a single-mode fiber that routes them to a grating spectrograph, and the resulting spectral interferograms are recorded with a CCD camera. The complex spectrum, i.e., amplitude and phase, is extracted from the interferogram (30). The reference beam is derived from the $\mathbf{k}_c$ beam before the sample and routed around the sample. A series of interferograms are recorded as a function of delay between $\mathbf{k}_a$ and $\mathbf{k}_b$. The delay between $\mathbf{k}_a$ and $\mathbf{k}_b$ is actively stabilized by using a servo loop that monitors the interference fringes of a copropagating HeNe laser beam. The servo loop is disabled and the interference signal is monitored while the delay changes. In addition, the delay between the reference beam and the $\mathbf{k}_c$ is actively stabilized by monitoring the spatial fringes between them. The details of the active stabilization have been described (31).

The spectra are $S(\omega_\tau, T, \omega_t)$, i.e., 2D Fourier transforms of $S(\tau, T, t)$ with respect to τ and t. The Fourier transform with respect to t is provided by the spectrometer. The Fourier transform with respect to τ is performed numerically. We use the phasor of the signal at ω_t to define the sign of the frequencies. Thus, for a rephasing sequence, ω_τ is negative, and these signals appear in the lower right quadrant of the (ω_t, ω_τ) plane. Nonrephasing signals appear in the upper right quadrant.

The phase of the signal is determined by the phase difference between the first two pulses and the phase of the third pulse, plus any phase shifts produced by the physical processes in the sample. In semiconductors, many-body interactions produce phase shifts; thus, determination of the signal phase provides important information. Although $S(\omega_\tau, T, \omega_t)$ is complex, the as-measured spectra have an arbitrary overall phase rotation that must be corrected before a separation into real and imaginary components is meaningful. The arbitrary phase comes from the unknown phase difference between the first two pulses at zero delay and from the unknown phase shift between the reference beam and third pulse. To correct for these shifts, we perform an auxiliary spectrally resolved differential transmission (SRDT) experiment (32). A phase rotation is applied to $S(\tau = 0, T, \omega_t)$ until the real part matches the SRDT signal for a delay T between the pump and probe pulses. The phase rotation that gives the best match is then applied to all of the interferograms. Because semiconductors exhibit strong dependence on the excitation level, it is important to match the excitation powers in the SRDT measurement to those used to acquire the 2D spectrum.

The sample is a 10-period GaAs /$Al_{0.3}Ga_{0.7}As$ multiple quantum well with 10-nm wells and 10-nm barriers. The heterostructure is grown by molecular beam epitaxy. The sample is affixed to a sapphire plate and the substrate is removed by lapping and etching. The sample is held at 8 K in a cold-finger continuous flow cryostat. The absorption spectrum displays prominent heavy-hole (hh) and light-hole (lh) exciton resonances with excitonic-binding energy of $\approx$10 meV. The spectral positions of the resonances are very sensitive to strain, because of both the difference in thermal coefficient of expansion between the sample and sapphire disk and mechanical strain imposed by mounting to the cold finger. As a consequence, the positions of the peaks vary slightly, although all spectra shown are from the same wafer. The incident pulses have sufficient bandwidth to excite both excitonic resonances and create unbound electron-hole pairs.

Theory. Calculations are performed by using a microscopic many-body theory (24). A 1D tight-binding model is used to make the numerical computations tractable. These calculations will not provide quantitative agreement with experiment; however, the qualitative features are reproduced. To isolate many-body effects and correlation terms, the calculations can include all coherent contributions to the third-order optical response or include only terms caused by first-order Coulomb interactions (i.e., Hartree–Fock) and neglecting the Coulomb interaction altogether, in which case the signal is caused by Pauli blocking.

In symbolic form, the equations of motion for the interband coherence, P, and the two-exciton amplitude, $\bar{B}$, are (22, 33–36):

$$-i\hbar\frac{\partial P}{\partial t} = \hbar(\omega_x - i\gamma)P + V_C P^* P P - V_C P^* \bar{B} + \mu^* E - \mu^* E P^* P,$$

$$-i\hbar\frac{\partial \bar{B}}{\partial t} = \hbar(\omega_B - i\beta)\bar{B} + V_C P P,$$

where $\hbar\omega_X$ is the exciton energy, $\hbar\omega_B$ is the biexciton energy, μ is the dipole moment of the optical transitions, γ and β are the phenomenological exciton and biexciton dephasing rates, respectively, and V_C is the Coulomb matrix that gives rise to the exciton and biexciton resonances and interaction between them. The microscopic version of these equations includes spatial indices of the tight-binding model and indices for the conduction, hh, and lh bands. Selection rules appropriate for dipole transitions in III–V semiconductors are used. Disorder can also be modeled as fluctuations of ω_X from site to site (37).

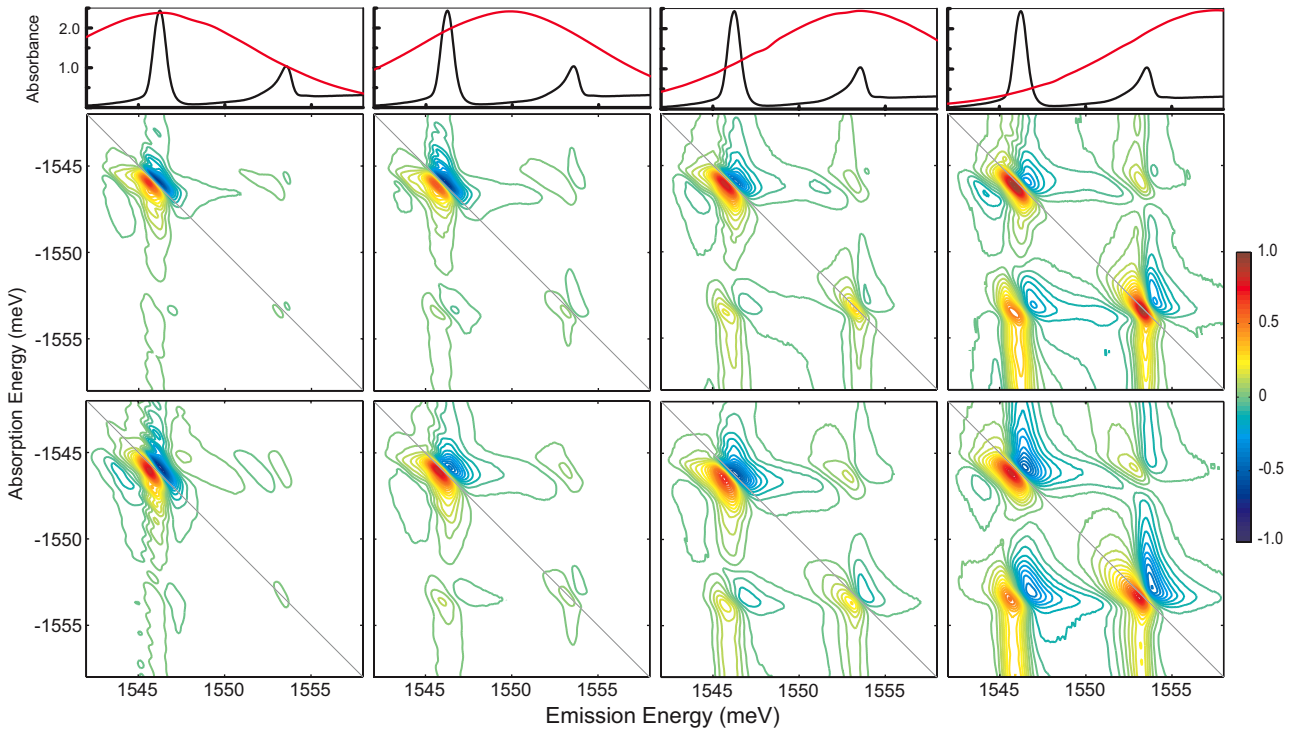

Fig. 2. Experimental real 2DFTS of a multiple quantum well for colinear-polarized excitation, $T = 200$ fs, and rephasing time ordering. For each tuning, the lower 2DFTS is taken at twice the power of the upper one. For reference, the linear absorption spectrum is overlaid on the laser spectrum at the top.

Results and Discussion

The 2DFTS of excitonic resonances is very sensitive to excitation conditions. These conditions include the spectrum of the incident laser pulses, their intensity, and their polarizations. Previous 2DFTS studies have used colinear-polarized excitation pulses, which is experimentally the most straightforward method but not the simplest to interpret. The earlier studies also only used a single tuning and power of the incident pulses, with the latter corresponding to a fairly high excitation density in the sample. Varying the laser tuning for colinear-polarized excitation shows that the theory qualitatively reproduces the experimental results for the real part of the 2DFTS. Cocircular-polarized excitation pulses provide the simplest case for isolating many-body effects as they are responsible for the coupling between the hh and lh exciton resonances, as confirmed by theoretical results. Cross-linear-polarized excitation suppresses one-exciton resonances and reveals contributions caused by biexcitons, again in agreement with theory.

Tuning Dependence for Colinear-Polarized Excitation. The sensitivity of the 2DFTS to the tuning of the incident laser pulses is shown in Fig. 2 where rephasing real spectra are shown for four tunings of the incident laser and colinear polarization of the excitation pulses. Furthermore, for each tuning, the results at two excitation densities, differing by a factor of two, are shown. The linear absorption spectrum and laser spectrum are shown above each pair of spectra. The lowest tuning corresponds to the peak of the laser spectrum coinciding with that of the hh exciton resonance. From there it is increased to be halfway between the hh and lh excitons, coincident with the lh exciton, and finally several meV above the lh exciton, which puts it well into the continuum of unbound electron-hh pairs. However, in all four cases, the laser bandwidth is sufficient so that both exciton resonances and unbound pairs are excited. Clearly, the relative strengths of the different features vary with tuning, a relatively straightforward effect caused by the changing excitation density due to spectral overlap.

All of the 2DFTS exhibit similar features. Two features occur on the diagonal at the photon energies of the hh and lh excitons. Both of these correspond to pathways that only involve one type of exciton. In addition, two features, known as "cross-peaks," are observed off the diagonal. They occur at the absorption photon energy of the lh exciton and emission photon energy of the hh exciton, and vice versa. Such cross-peaks are expected for colinear excitation as coupling occurs through the shared conduction band states. For the higher laser tunings, a vertical "stripe" is also apparent at the emission photon energies of both excitons. These stripes are clearly caused by excitation of unbound electron-hole pairs. If the continuum states acted as a set of inhomogeneously broadened transitions, they would appear in the 2DFTS as a diagonal feature, not vertical stripes. The stripes occur because free pairs strongly couple to the excitonic resonances, resulting in a dominant signal at the exciton (19). They have previously been observed in coherent excitation spectroscopy (38) and magnitude 2DFTS (23).

It is striking that the spectra display "dispersive" line shapes. A simple few-level model would produce "absorptive" lines, i.e., a simple positive peak centered at the exciton photon energies. Instead, we observe a line that is better described as the derivative of a peak in the cross-diagonal direction for rephasing spectra or the diagonal direction for nonrephasing spectra. Previous measurements found similar lineshapes and explained them in a phenomenological model as being caused by the dominance of many-body effects, in particular, the fact that the resonance frequencies depend on excitation level (11). In the phenomenological theory, the relative contribution of different many-body terms could be independently adjusted.

Calculations qualitatively reproduce the experimental structure of the spectra, the dispersive lineshapes, and the tuning dependence, as shown in Fig. 3. Realistic material parameters are chosen, including effective masses, dipole matrix elements, energetic offsets, and Coulomb interaction, based on matching the experimental absorption spectrum. The experimental conditions, such as pulse

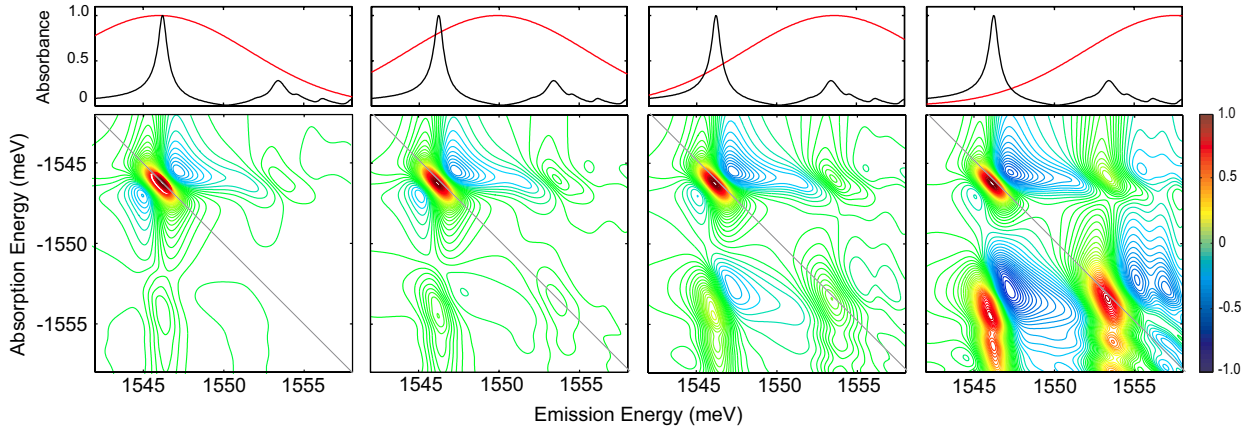

Fig. 3. Theoretical real 2DFTS for colinear-polarized excitation, $T = 200$ fs and 0.7 meV inhomogeneous broadening as a function of tuning. The calculated linear absorption spectrum overlaid with the laser spectrum is shown at the top.

duration, tuning, and polarization, are incorporated into the model. The dephasing times are taken as phenomenological parameters and adjusted to give agreement with the experimental 2DFTS. The many-body contributions are intrinsic in this theory, and their relative strengths cannot be adjusted. Good qualitative agreement with the experimental real 2DFTS is obtained, including the tuning dependence, showing that the theory accurately captures the many-body processes. The theory applies to weak excitation, thus the dispersive character seen in the experimental data for excitation at the hh exciton and for larger intensity must be caused by effects beyond third order in the electric field of the incident pulses. The relative strengths of the various lines depend strongly on the dephasing rates of the excitonic resonances.

Cocircular-Polarized Excitation and Dominance of Many-Body Contributions. Although colinear-polarized excitation is the most straightforward experimentally, it is not optimum for revealing many-body contributions. Cocircular-polarized excitation, on the other hand, provides an immediate and striking demonstration of the dominant role that many-body processes play. Based on the magnetic substates for the valence and conduction bands, no coupling between hh and lh excitons would be expected for cocircular excitation. Previous TFWM (39), SRDT (40), and coherent excitation spectroscopy (38) studies have shown that indeed coupling does occur for cocircular excitation pulses, attributing it to many-body correlations. Experimental real rephasing and nonrephasing 2DFTS for cocircular excitation are shown in Fig. 4. The clear cross-peaks between the hh and lh excitons demonstrate that they are indeed coupled because of many-body effects.

To verify that many-body effects are responsible for the cross-peaks, we performed calculations for three cases, as shown in Fig. 5. If only Pauli-blocking terms are included (i.e., the Coulomb interaction is neglected except for the electron-hole attraction and the optical nonlinearity arises from the saturation of the resonances by band filling) no cross-peaks occur, and the continuum states appear on the diagonal. When the Coulomb interaction is included, but only within a Hartree–Fock approximation, weak cross-peaks appear, but the relative strengths of the cross-peaks and diagonal peaks do not agree with the experiment. Additionally, the continuum states display cross-peaks, but no vertical feature, as occurs in the experiment. Only the full theory, including correlation terms beyond Hartree–Fock, provides good agreement with the experiment. The full theory reproduces the relative strengths of the peaks, with the off-diagonal peak at the lh exciton absorption photon energy and hh exciton emission photon energy dominating. Furthermore, the continuum contribution is now vertical stripes at the exciton emission photon energies.

Enhancement of low-energy resonances can also occur because of incoherent relaxation. As incoherent relaxation occurs when the system is in a population state, it is can be probed by varying T (16). Fig. 4 shows real 2DFTS for both $T = 100$ fs and $T = 2$ ps. Although there is some strengthening of the emission at the hh exciton photon energy, it is not large. Thus, we conclude that the dominance of the hh exciton emission is not caused by incoherent relaxation. The theory is within the coherent limit, so incoherent relaxation is not considered. The good agreement provided by the coherent limit further supports the conclusion that incoherent relaxation is not significant for spectra taken with T of a few hundred fs.

Biexcitonic Contributions to Cross-Linear-Polarized Excitation. The contribution of bound biexcitonic states to TFWM signals has proven to be difficult to isolate because the biexciton-binding

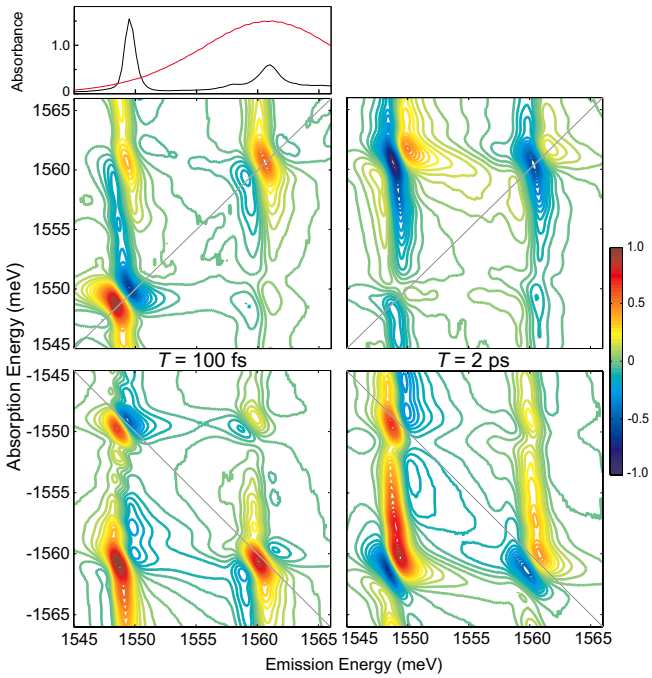

Fig. 4. Experimental real ZDFTS for cocircular-polarized excitation of a multiple quantum well. Both rephasing (*Bottom*) and nonrephasing (*Middle*) are shown for $T = 100$ fs and $T = 2$ ps (*Right*). (*Top*) The linear absorption and laser spectrum are shown.

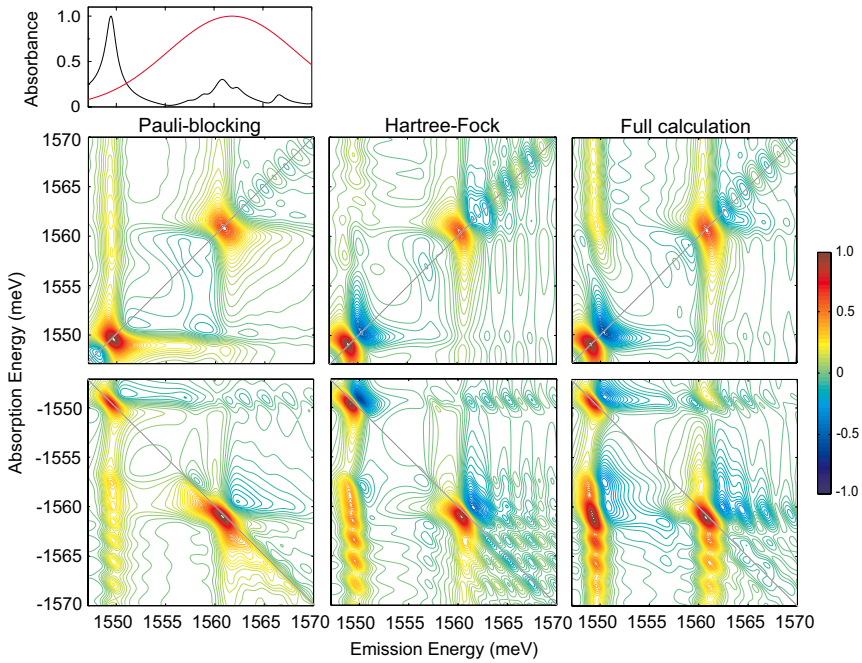

Fig. 5. Theoretical real ZDFTS for cocircular excitation of a multiple quantum well. Both rephasing (*Bottom*) and nonrephasing (*Middle*) cases are shown including only Pauli-blocking (*Left*), within the Hartree-Fock approximation (*Center*), and for the full calculation including all correlation terms that contribute up to third order in the electric field (*Right*) for cocircular-polarized excitation at $T = 100$ fs. (*Top*) The calculated linear absorption and laser spectrum are shown.

energy is small and often inhomogeneity results in broadening of a comparable amount. The best evidence has been the presence of beats with a frequency corresponding to the biexciton binding energy for "negative" delays (5) or mediated by strong inhomogeneous broadening (41). Biexcitonic effects are often more apparent for cross-linear-polarized excitation because of the suppression of excitation-induced many-body terms that dominate the one-exciton resonances for colinear polarization.

Fig. 6 shows experimental and theoretical magnitude 2DFTS spectra for cross-linear-polarized excitation pulses, where the first two pulses are cross-polarized. Currently, we cannot produce real 2DFTS when the first two pulses are cross-polarized because the auxiliary experiment used to determine the overall phase is no longer valid. Thus we only plot magnitude spectra.

Both experimental and theoretical spectra show horizontal elongation of the peaks. This elongation of the peaks is caused by emission at the exciton-to-biexciton transition. The elongation is missing for calculations that neglect two-exciton states (25). This contribution can be isolated by using appropriate combinations of circularly polarized pulses. In addition, two quantum pathways that go through a nonradiative coherence between the ground state and the biexciton can be isolated in experiments where all three excitation pulses are phase-locked (25).

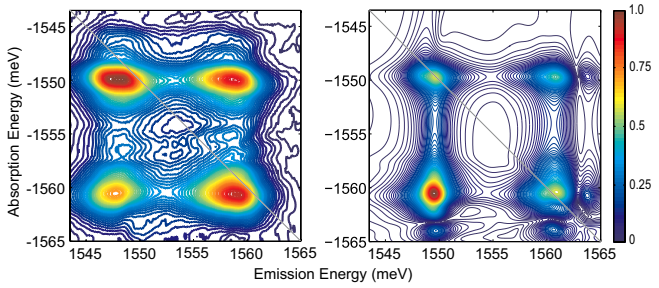

Fig. 6. Experimental (*Left*) and theoretical (*Right*) magnitude 2DFTS for cross-linear polarization of the first and second excitation beams.

Conclusions

Optical 2DFTS is proving to be a powerful method for studying many-body interactions among optically created excitations in semiconductors. 2DFTS is able to separate out specific pathways and phase-resolve the signal. The combination of these capabilities gives a much more stringent test of the theory and allows for the identification of specific effects. Comparison to theory clearly demonstrates the essential role of many-body effects and that only a full theory, including correlation terms beyond Hartree–Fock, is correct. The influence of the band structure on this signal needs to be the subject of further numerical simulations.

The results presented here only begin to explore the full richness of this technique. Many interesting avenues of investigation remain such as the dependence on T, alternate spectra such as $S(T, \omega_T, \omega_t)$ (25), alternate time ordering, and the dependence of the 2DFTS on excitation density.

We thank S. Mukamel and A. D. Bristow for discussions and T. Harvey for technical assistance. The work at JILA is supported by the Chemical Sciences, Geosciences, and Energy Biosciences Division, Office of Basic Energy Science, Office of Science, U.S. Department of Energy. The work at Marburg is supported by the Optodynamics Center of the Philipps-University Marburg, the Deutsche Forschungsgemeinshaft, and the John von Neumann Institut für Computing, Forschungszentrum Jülich, Germany. T.M. was supported by the Deutsche Forschungsgemeinshaft through Heisenberg Fellowship ME 1916/1.

1. Haug H, Koch, SW (2004) *Quantum Theory of the Optical and Electronic Properties of Semiconductors* (World Scientific, Singapore).
2. Chemla DS, Shah J (2001) *Nature* 411:549–557.
3. Leo K, Wegener M, Shah J, Chemla DS, Göbel EO, Damen TC, Schmitt-Rink S, Schäfer W (1990) *Phys Rev Lett* 65:1340–1343.
4. Wegener M, Chemla DS, Schmitt-Rink S, Schäfer W (1990) *Phys Rev A* 42:5675–5683.
5. Bott K, Heller O, Bennhardt D, Cundiff ST, Thomas P, Mayer EJ, Smith GO, Eccleston R, Kuhl J, Ploog K (1993) *Phys Rev B* 48:17418–17426.
6. Wang H, Ferrio K, Steel DG, Hu YZ, Binder R, Koch SW (1993) *Phys Rev Lett* 71:1261–1264.
7. Hu YZ, Binder R, Koch SW, Cundiff ST, Wang H, Steel DG (1994) *Phys Rev B* 49:14382–14386.

8. Shacklette JM, Cundiff ST (2002) *Phys Rev B* 66:045309.
9. Kim DS, Shah J, Damen TC, Schäfer W, Jahnke F, Schmitt-Rink S, Köhler K (1992) *Phys Rev Lett* 69:2725–2728.
10. Weiss S, Mycek M-A, Bigot J-Y, Schmitt-Rink S, Chemal DS (1992) *Phys Rev Lett* 69:2685–2688.
11. Li X, Zhang T, Borca CN, Cundiff ST (2006) *Phys Rev Lett* 96:057406.
12. Ernst RR, Bodenhausen G, Wokaun A (1987) *Principles of Nuclear Magnetic Resonance in One and Two Dimensions* (Oxford Science, New York).
13. Mukamel S (2000) *Annu Rev Phys Chem* 51:691–729.
14. Hybl JD, Ferro AA, Jonas DM (2001) *J Chem Phys* 115:6606–6622.
15. Jonas DM (2003) *Annu Rev Phys Chem* 54:425–463.
16. Brixner T, Stenger J, Vaswani HM, Cho M, Blankenship RE, Fleming GR (2005) *Nature* 434:625–628.
17. Koch M, Feldmann J, von Plessen G, Göbel EO, Thomas P, Köhler K (1992) *Phys Rev Lett* 69:3631–3634.
18. Lyssenko VG, Erland J, Balsev I, Pantke K-H, Rasbirin BS, Hvam J (1993) *Phys Rev B* 48:5720–5723.
19. Cundiff ST, Koch M, Knox WH, Shah J, Stolz W (1996) *Phys Rev Lett* 77:1107–1110.
20. Euteneuer A, Finger E, Hofmann M, Stolz W, Meier T, Thomas P, Koch SW, Rühle W, Hey R, Ploog K (1999) *Phys Rev Lett* 83:2073–2076.
21. Sieh C, Meier T, Jahnke F, Knorr A, Koch SW, Brick P, Hübner M, Ell C, Prineas J, Khitrova G, Gibbs HM (1999) *Phys Rev Lett* 82:3112–3115.
22. Sieh C, Meier T, Knorr A, Jahnke F, Thomas P, Koch SW (1999) *Eur Phys J B* 11:407–421.
23. Borca CN, Zhang T, Li X, Cundiff ST (2005) *Chem Phys Lett* 416:311–315.
24. Kuznetsova I, Thomas P, Meier T, Zhang T, Li X, Mirin RP, Cundiff ST (2007) *Solid State Commun* 142:154–158.
25. Yang L, Schweigert IV, Cundiff ST, Mukamel S (2007) *Phys Rev B* 75:125302.
26. Bigot JY, Mycek M-A, Weiss S, Ulbrich RG, Chemla DS (1993) *Phys Rev Lett* 70:3307–3310.
27. Chen X, Walecki WJ, Buccafusca O, Fittinghoff DN, Smirl AL (1997) *Phys Rev B* 56:9738–9743.
28. Likforman JP, Joffre M, ThierryMieg V (1997) *Opt Lett* 22:1104–1106.
29. Khalil M, Demirdöven N, Tokmakoff A (2003) *Phys Rev Lett* 90:047401.
30. Lepetit L, Chèriaux G, Joffre M (1995) *J Opt Soc Am B* 12:2467–2474.
31. Zhang T, Borca CN, Li X, Cundiff ST (2005) *Opt Express* 13:7432–7441.
32. Faeder SMG, Jonas DM (1999) *J Phys Chem A* 103:10489–10505.
33. Meier T, Thomas P, Koch SW (2007) *Coherent Semiconductor Optics: From Basic Concepts to Nanostructure Applications* (Springer, Berlin).
34. Axt VM, Stahl A (1994) *Z Phys B* 93:195–204.
35. Axt VM, Stahl A (1994) *Z Phys B* 93:205–211.
36. Lindberg M, Hu YZ, Binder R, Koch SW (1994) *Phys Rev B* 50:18060.
37. Weiser S, Meier T, Möbius M, Euteneuer A, Mayer EJ, Stolz W, Hofmann M, Rühle WW, Thomas P, Koch SW (2000) *Phys Rev B* 61:13088–13098.
38. Finger E, Kraft SP, Hofmann M, Meier T, Koch SW, Stolz W, Rühle WW (2002) *Phys Stat Sol B* 234:424–434.
39. Smirl AL, Stevens ML, Chen X, Buccafusca O (1999) *Phys Rev B* 60:8267–8275.
40. Donovan MW, Schülzgen A, Lee J, Blanche P-A, Peyhambarian N, Khitrova G, Gibbs HM, Rumyantsev I, Kwong NH, Takayam R, *et al.* (2001) *Phys Rev Lett* 87:237402.
41. Albrecht TF, Bott K, Meier T, Schulze A, Koch M, Cundiff ST, Feldmann J, Stolz W, Thomas P, Koch SW, Göbel EO (1996) *Phys Rev B* 54:4436–4439.